AGU PUBLICATIONS

Geophysical Research Letters

RESEARCH LETTER
10.1002/2015GL065889

Key Points:
- Temperature feedbacks are investigated in simple column models
- Opposing lapse rate responses at high and low latitudes are analyzed
- Regional differences in lapse rate response result in polar amplification

Correspondence to:
A. E. Payne,
aepayne@uci.edu

Citation:
Payne, A. E., M. F. Jansen, and T. W. Cronin (2015), Conceptual model analysis of the influence of temperature feedbacks on polar amplification, *Geophys. Res. Lett.*, *42*, 9561–9570, doi:10.1002/2015GL065889.

Received 21 AUG 2015
Accepted 22 OCT 2015
Published online 14 NOV 2015

Conceptual model analysis of the influence of temperature feedbacks on polar amplification

Ashley E. Payne[1], Malte F. Jansen[2], and Timothy W. Cronin[3]

[1]Department of Earth System Science, University of California, Irvine, California, USA, [2]Department of the Geophysical Sciences, The University of Chicago, Chicago, Illinois, USA, [3]Department of Earth and Planetary Sciences, Harvard University, Cambridge, Massachusetts, USA

Abstract The role of temperature feedbacks in polar amplification of climate change is examined by comparing the response of idealized high- and low-latitude atmospheric columns to greenhouse gas forcing. An analytic expression for the surface polar amplification factor is derived with a one-layer atmospheric model and compared to a more detailed column model with two radiative transfer schemes. The modeled temperature profiles result from competition between the stabilizing influences of atmospheric heat flux convergence and atmospheric solar heating (dominant at high latitudes), and the destabilizing influence of surface solar heating (dominant at low latitudes). For a stable high-latitude radiative-advective atmosphere, the lapse rate increases with greenhouse gas forcing, leading to a positive feedback, and is dependent on the nature of the forcing—pointing to limitations of the traditional forcing-feedback framework. For a low-latitude radiative-convective atmosphere, the lapse rate decreases, leading to a negative feedback.

1. Introduction

Surface temperatures in the Arctic have increased at twice the rate of the global average [*Meehl et al.*, 2007]. The strengthened response of surface warming at high latitudes is referred to as polar amplification. The surface albedo feedback, or absorption of more shortwave radiation with warming due to ice loss, is thought to play a large role in present-day polar amplification [*Manabe and Wetherald*, 1975; *Screen and Simmonds*, 2010]. However, this positive feedback cannot fully explain polar amplification in idealized model simulations and in paleoclimate records of both natural and forced climate variability where albedo feedbacks are reduced or absent [*Held*, 1978; *Manabe and Stouffer*, 1980; *Hall*, 2004; *Winton*, 2006; *Miller et al.*, 2010; *Roe et al.*, 2015]. The additional feedbacks that contribute to polar amplification can be difficult to analyze because they interact not only with the surface albedo feedback but also with changes in atmospheric [*Graversen et al.*, 2008; *Yang et al.*, 2010] and oceanic [*Chylek et al.*, 2009] energy transport.

A large fraction of polar amplification can be attributed to longwave radiative feedbacks [*Winton*, 2006], which include the effects of clouds [*Vavrus*, 2004], water vapor [*Graversen and Wang*, 2009], and temperature [*Pithan and Mauritsen*, 2014]. Longwave temperature feedbacks can be further broken down into the Planck feedback, or change in outgoing radiation due to vertically uniform warming, and the lapse rate feedback, or change in outgoing radiation due to deviations from vertically uniform warming. Recent work has highlighted the lapse rate feedback as a possible driver of polar amplification due to its differing response between high and lower latitudes [*Lu and Cai*, 2010; *Bintanja et al.*, 2011; *Pithan and Mauritsen*, 2014; *Graversen et al.*, 2014]. However, it is difficult to consider the lapse rate feedback independently within a global model [*Graversen et al.*, 2014], and the basic controls on the high-latitude lapse rate and its sensitivity to climate remain poorly understood. A simplified method is needed to better understand high-latitude lapse rate changes and their role in polar amplification.

We use a hierarchy of conceptual models to isolate the lapse rate feedback and investigate how it contributes to polar amplification. We analyze the response of two climate regimes: (1) convectively stable, high-latitude (HL) radiative-advective equilibrium (small surface solar absorption and large net atmospheric heating) and (2) convectively neutral, low-latitude (LL) radiative-convective equilibrium (large surface solar absorption and small net atmospheric heating). We examine the sensitivity of surface temperature to varying surface solar absorption, atmospheric heating, and total longwave optical depth of the atmosphere. For both a simple

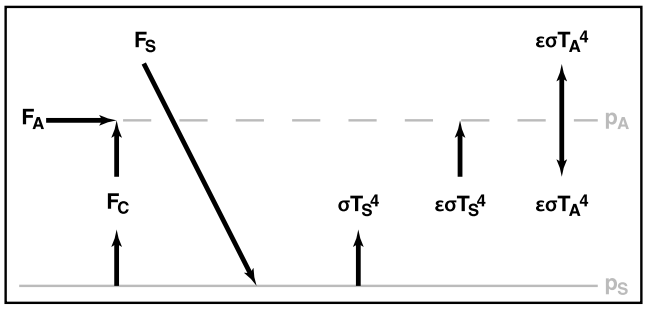

Figure 1. Illustration of a simple one-layer energy balance model with a surface (p_S = 1000 hPa) and an atmospheric layer (p_A = 500 hPa). F_S is the shortwave radiation absorbed by the surface, F_A is the sum of advective heat transport due to dynamics and atmospheric absorption of shortwave radiation, F_C is vertical convective heat transport, T_S is the temperature of the surface, T_A is the temperature of the atmospheric layer, ϵ is the atmospheric emissivity, and σ is the Stefan-Boltzmann constant.

single-layer atmosphere and a more detailed dry column model of the atmosphere, we find that the lapse rate feedback amplifies the high-latitude surface temperature response to changing greenhouse gas concentrations. We conclude with a brief investigation of how inclusion of the water vapor feedback modifies our results.

2. Methods

We use the following two models: (1) a simple two-level, one-dimensional energy balance model (EBM) and (2) a 26-layer column model, based on the Climate Modelling and Diagnostics Toolkit [*Caballero et al.*, 2013]. In the EBM, the lower level represents the surface (p_S = 1000 hPa, T_S) and the upper level represents the midtroposphere (p_A = 500 hPa, T_A), referred to as the "atmosphere" (Figure 1 shows a schematic of model inputs). Equilibrium implies energy balance at both levels:

$$0 = F_S - F_C + \epsilon\sigma T_A^4 - \sigma T_S^4, \qquad \text{(surface)} \tag{1}$$

$$0 = F_A + F_C + \epsilon\sigma T_S^4 - 2\epsilon\sigma T_A^4, \qquad \text{(atmosphere)} \tag{2}$$

where ϵ is the atmospheric emissivity, σ is the Stefan-Boltzmann constant, and T_S and T_A are the surface and atmospheric temperatures, respectively. Equations (1) and (2) include F_C to account for vertical convective heat transport. Convection is triggered when $(T_S - T_A)$ exceeds a temperature-dependent convective lapse rate, Δ_T, defined as the vertical temperature difference in units of K. Δ_T is computed in the EBM by following a moist adiabat from p_S to p_A. For current low-latitude surface temperatures, $\Delta_T \approx 31$ K, and Δ_T decreases with warming by $\gamma \equiv d\Delta_T/dT_s \approx -0.6$ K/K. A current high-latitude $T_S = 260$ K gives a $\Delta_T^{HL} \approx 44$ K—larger than any of our high-latitude EBM solutions.

We use Δ_T and the top-of-atmosphere energy balance to solve for the low-latitude surface and atmospheric temperatures in the EBM:

$$F_S + F_A = (1-\epsilon)\sigma T_S^4 + \epsilon\sigma(T_S - \Delta_T)^4, \tag{3}$$

$$T_A = T_S - \Delta_T. \tag{4}$$

We use $F_C = 0$ to solve for the high-latitude T_S and T_A:

$$\sigma T_S^4 = \frac{2F_S + F_A}{(2-\epsilon)}, \tag{5}$$

$$\sigma T_A^4 = \frac{\epsilon F_S + F_A}{\epsilon\,(2-\epsilon)}, \tag{6}$$

which is physical so long as the column is convectively stable, that is $T_S - T_A < \Delta_T$ [see also *Abbot and Tziperman*, 2009].

The energy sources are F_S, which represents the surface shortwave absorption (LL: 215.1 W m^{-2}, HL: 34.9 W m^{-2}), and F_A, which represents the sum of atmospheric heat flux convergence (LL: −64.2 W m^{-2}, HL: 100.8 W m^{-2}) and direct atmospheric shortwave absorption (LL: 90.9 W m^{-2}, HL: 40.2 W m^{-2}). Values for these energy sources for representative low-latitude (zonal mean from 10° to 15°N) and high-latitude (zonal mean from 80° to 85°N) regions are derived from climatological (1979–2015) averages from Modern-Era Retrospective Analysis for Research and Applications (MERRA) reanalysis [*Rienecker et al.*, 2011]. In general, F_S should also account for both ocean heat flux convergence and subsurface heat storage. We neglect ocean heat flux convergence because it is small in both regions [*Trenberth and Caron*, 2001; *Serreze et al.*, 2007]. We also neglect subsurface heat storage because we focus on annual mean conditions; applying the model to understand seasonal warming patterns would require including surface heat storage in F_S.

The column model equivalent of the EBM uses a grey gas radiative scheme coupled to a slab ocean and simple turbulence and convection schemes. Turbulence is parameterized using a bulk formula for surface sensible heat exchange and weak vertical diffusion of potential temperature (diffusivity, $\kappa = 0.02\ \mathrm{m^2 s^{-1}}$). Convection is parameterized by hard adjustment to the moist adiabatic lapse rate. The influence of greenhouse gases on surface and atmospheric temperatures is represented in the EBM by the atmospheric emissivity, ϵ ($0 < \epsilon <= 1$), and in the grey gas column model by the optical depth, $\tau = \tau_0(1-p/p_S)^2$ (where τ_0 is the total column optical depth). A water vapor feedback is not incorporated into either model.

In a second configuration of the column model, we use a multiband radiative scheme based on the Column Radiation Model by National Center for Atmospheric Research's Community Climate Model (CCM3). In this configuration, the ozone profile is taken from MERRA reanalysis, the model is forced by annually averaged insolation (LL: 411.9 W m^{-2}, HL: 179.0 W m^{-2}), and F_A is limited to the contribution from meridional heat flux convergence (the radiative scheme calculates shortwave atmospheric absorption). The surface albedo is adjusted (LL: 0.11, HL: 0.53) so that temperature profiles approximate reanalysis (averaged from 2010 to 2015) with $p\mathrm{CO}_2$ = 400 ppmv. We run this model with both fixed specific humidity (fixed q) and fixed relative humidity (fixed RH) to examine the role of temperature and water vapor feedbacks.

In both the grey gas and CCM3 models, atmospheric heat flux convergence is parameterized following a square-root distribution:

$$Q(p) = \frac{3F_A}{2(p_S - p_T)}\left[\frac{(p-p_T)}{(p_S-p_T)}\right]^{1/2} \tag{7}$$

going to zero at the tropopause (p_T^{LL} = 90 hPa and p_T^{HL} = 275 hPa) (roughly approximating the tropospheric heat transport profile shown in *Oort* [1974]).

3. Theory

We start with an analytic investigation of the EBM's sensitivity of surface temperatures to (1) small changes in atmospheric emissivity ($\delta T_S/\delta\epsilon$) and to (2) fixed-flux forcing ($\delta T_S/\delta F$), where F represents either radiative forcing or advective heat flux convergence. We focus on the two representative climate regimes described above to explore differences between high and low latitudes.

3.1. Sensitivity to Emissivity

To analyze the response of surface temperatures to a small change in the atmospheric emissivity, we substitute $\epsilon + \delta\epsilon$ and $T_S + \delta T_S$ for ϵ and T_S, respectively, into the EBM (equations (3) and (5)). Note that in the real climate system, both local feedbacks and changes in heat transport would also alter F_S and F_A; our simplifying assumption of constant F_S and F_A is intended to isolate the role of temperature feedbacks. For infinitesimal δT_S and $\delta\epsilon$, this yields for low-latitude (δT_S^{LL}) and high-latitude (δT_S^{HL}) surface temperature change:

$$\delta T_S^{\mathrm{LL}} = \frac{T_S^4 - (T_S - \Delta_T)^4}{4(1-\epsilon)T_S^3 + 4\epsilon(1-\gamma)(T_S-\Delta_T)^3}\delta\epsilon, \tag{8}$$

$$\delta T_S^{\mathrm{HL}} = \frac{T_S}{4(2-\epsilon)}\delta\epsilon. \tag{9}$$

Assuming that the low-latitude lapse rate, Δ_T, is much smaller than T_S, we can simplify equation (8) to

$$\delta T_S^{\mathrm{LL}} \approx \frac{\Delta_T}{1-\epsilon\gamma}\delta\epsilon. \tag{10}$$

Equation (9) shows that δT_S^{HL} is proportional to the high-latitude surface temperature and increases with emissivity. Equation (10) shows that δT_S^{LL} depends on Δ_T and its sensitivity to temperature, γ. Assuming equal changes in emissivity, we can estimate a polar amplification factor using equations (9) and (10):

$$\frac{\delta T_S^{HL}}{\delta T_S^{LL}} \approx \frac{(1-\epsilon\gamma)T_S^{HL}}{4(2-\epsilon)\Delta_T}. \tag{11}$$

For $\Delta_T \approx 33$ K, $\gamma \approx -0.6$, and $\epsilon = 0.9$, we find a polar amplification factor of roughly 2.6. Note that this factor is an approximation because higher-order terms in equation (8) are omitted in equation (10); exact calculation by dividing equation (9) by equation (8) gives a polar amplification factor of 2.2. Note also that equation (11) could be multiplied by $\delta\epsilon^{HL}/\delta\epsilon^{LL}$ to account for unequal changes in emissivity due to meridional variation in the water vapor feedback.

The polar amplification in the EBM results from the differing lapse rate response and cannot be attributed simply to the differing Planck feedback. In the scenario of a fixed lapse rate (equation (10) with $\gamma = 0$), the temperature response depends to first order only on the lapse rate itself and is independent of T_S. Therefore, at the same fixed lapse rate, colder high-latitude surface temperatures alone would not lead to polar amplification in response to atmospheric emissivity changes. Considering this scenario from a forcing-feedback perspective, a weaker Planck feedback at cold high latitudes would be offset by a similarly weaker radiative forcing.

3.2. Sensitivity to Forcing

The sensitivity to a unit forcing of 1 W m^{-2} allows us to calculate Planck and lapse rate feedback parameters for the atmosphere in each region and to determine whether the feedbacks depend on the type of forcing. We investigate the sensitivity of surface temperature to three types of forcing: surface-based ($\delta T_S/\delta F_S$), atmospheric ($\delta T_S/\delta F_A$), and emissivity-induced radiative forcings ($\delta T_S/\delta F_R$). Here δF_R is the change in top-of-atmosphere energy balance due to a small change in atmospheric emissivity, holding T_S and T_A fixed

$$\delta F_R \equiv (\sigma T_S^4 - \sigma T_A^4)\delta\epsilon. \tag{12}$$

The radiative forcing from an increase in atmospheric emissivity (due to greenhouse gases) depends on the difference between surface and atmospheric temperature—larger at low latitudes than high latitudes. The radiative forcing for our two representative columns is given by

$$\delta F_R^{LL} = \left[\sigma T_S^4 - \sigma(T_S - \Delta_T)^4\right]\delta\epsilon, \tag{13}$$

$$\delta F_R^{HL} = \left[\frac{\sigma T_S^4}{2} - \frac{F_A}{2-\epsilon}\left(\frac{1}{\epsilon} - \frac{1}{2}\right)\right]\delta\epsilon. \tag{14}$$

We focus first on the sensitivity of T_S to forcing in low-latitude radiative-convective equilibrium. We perturb equation (3) to determine sensitivity of T_S to surface and atmospheric forcing and divide equation (8) by equation (13) to determine the sensitivity of T_S to emissivity-induced radiative forcing; all three sensitivities turn out to be equal:

$$\frac{\delta T_S^{LL}}{\delta F_S} = \frac{\delta T_S^{LL}}{\delta F_A} = \frac{\delta T_S^{LL}}{\delta F_R} = \frac{1}{4\sigma T_S^3(1-\epsilon) + 4\epsilon\sigma(1-\gamma)(T_S - \Delta_T)^3}. \tag{15}$$

The negative inverse of equation (15) gives the total feedback of the column, which, in this simplified model framework, is only a temperature feedback: $\lambda_T = -\delta F/\delta T_S$. This temperature feedback in turn can be broken into Planck and lapse rate components:

$$\begin{aligned} \lambda_P^{LL} &= -4\sigma\left[(1-\epsilon)T_S^3 + \epsilon(T_S - \Delta_T)^3\right] \\ \lambda_{LR}^{LL} &= 4\sigma\epsilon\gamma(T_S - \Delta_T)^3, \end{aligned} \tag{16}$$

where the Planck feedback (λ_P) is the response to a vertically uniform warming and the lapse rate feedback is the residual of $\lambda_T - \lambda_P$. Low-latitude feedbacks are independent of the type of forcing, and because the moist convective lapse rate decreases with temperature ($\gamma < 0$), the low-latitude lapse rate feedback is negative.

For high-latitude radiative-advective equilibrium, we perform a similar analysis: we perturb equation (5) to determine the sensitivity of T_S to F_S or F_A and divide equation (9) by equation (14) to determine the sensitivity of T_S to F_R:

$$\frac{\delta T_S^{\mathrm{HL}}}{\delta F_S} = \frac{1}{4\sigma T_S^3\left(1-\frac{\epsilon}{2}\right)}, \tag{17}$$

$$\frac{\delta T_S^{\mathrm{HL}}}{\delta F_A} = \frac{1}{8\sigma T_S^3\left(1-\frac{\epsilon}{2}\right)}, \tag{18}$$

$$\frac{\delta T_S^{\mathrm{HL}}}{\delta F_R} = \frac{1}{4\sigma T_S^3\left(1-\frac{\epsilon}{2}\right)-\frac{4F_A}{T_S}\left(\frac{1}{\epsilon}-\frac{1}{2}\right)}. \tag{19}$$

These sensitivities all differ from each other. The sensitivity of surface temperature to surface forcing is exactly double that to atmospheric forcing (previously noted by *Abbot and Tziperman* [2009]), and the sensitivity of surface temperature to emissivity-induced radiative forcing is larger still (the second term in the denominator of equation (19) reveals that $\delta T_S^{\mathrm{HL}}/\delta F_R$ is always increased relative to $\delta T_S^{\mathrm{HL}}/\delta F_S$ because $F_A > 0$). Note that the emissivity-induced radiative forcing will be negative if the surface is colder than the atmosphere ($T_S < T_A$), but the surface temperature nonetheless increases with increasing emissivity.

The Planck feedback is given by the same expression $\lambda_P = -4\sigma\left[(1-\epsilon)T_S^3 + \epsilon T_A^3\right]$ regardless of forcing. Therefore, one can interpret the differing sensitivity to forcing of the high-latitude equilibrium as arising from differences in the lapse rate response. The fixed Planck feedback, along with the total temperature feedback from equations (17)–(19) ($\lambda_T = -\delta F/\delta T_S$), allows us to calculate the forcing-specific lapse rate feedbacks:

$$\lambda_{\mathrm{LR}}^{\mathrm{HL}}(F_S) = 4\sigma\epsilon\left(T_A^3 - \frac{T_S^3}{2}\right), \tag{20}$$

$$\lambda_{\mathrm{LR}}^{\mathrm{HL}}(F_A) = -4\sigma\left(T_S^3 - \epsilon T_A^3\right), \tag{21}$$

$$\lambda_{\mathrm{LR}}^{\mathrm{HL}}(F_R) = 4\sigma\epsilon\left(T_A^3 - \frac{T_S^3}{2}\right) + \frac{4F_A}{T_S}\left(\frac{1}{\epsilon}-\frac{1}{2}\right). \tag{22}$$

The sign of the lapse rate feedback differs across forcings. It can be shown from equations (20) to (22) that the lapse rate feedback is always positive for surface forcing or radiative forcing and always either negative or zero for atmospheric heat flux forcing. The differences among equations (17)–(19) and (20)–(22) point to limitations of the conventional forcing-feedback analysis framework for understanding climate change at high latitudes. Changes in the lapse rate depend on the nature of the forcing, rather than depending solely on the surface temperature.

4. Model Results

Next, we compare predictions in section 3 to solutions of both the EBM and the grey gas column model over a range of emissivities and optical depths. In Figures 2a and 2b, we show high-latitude (blue) and low-latitude (orange) surface and atmospheric temperatures. Both models show polar amplification consistent with the analytical approximation in equation (11). The high-latitude surface temperature response is amplified by a factor of 2.2 in the EBM (near $\epsilon = 0.9$) and by 2.2 in the grey gas model (near $\tau_0 = 2.7$, chosen so that the low-latitude lapse rate is similar to the EBM). The increased sensitivity of high-latitude surface temperatures is attributable to the net atmospheric heat import, which stabilizes the atmosphere to convection and allows radiative forcing to drive the lapse rate toward a convectively neutral state. Both models agree on the magnitude of the lapse rate increase at high latitudes and decrease at low latitudes (dashed versus solid lines in Figure 2c). Changes in lapse rate with increasing optical depth lead to a positive feedback at high latitudes but a negative feedback at low latitudes. At low optical depth, the high-latitude lapse rate response in both

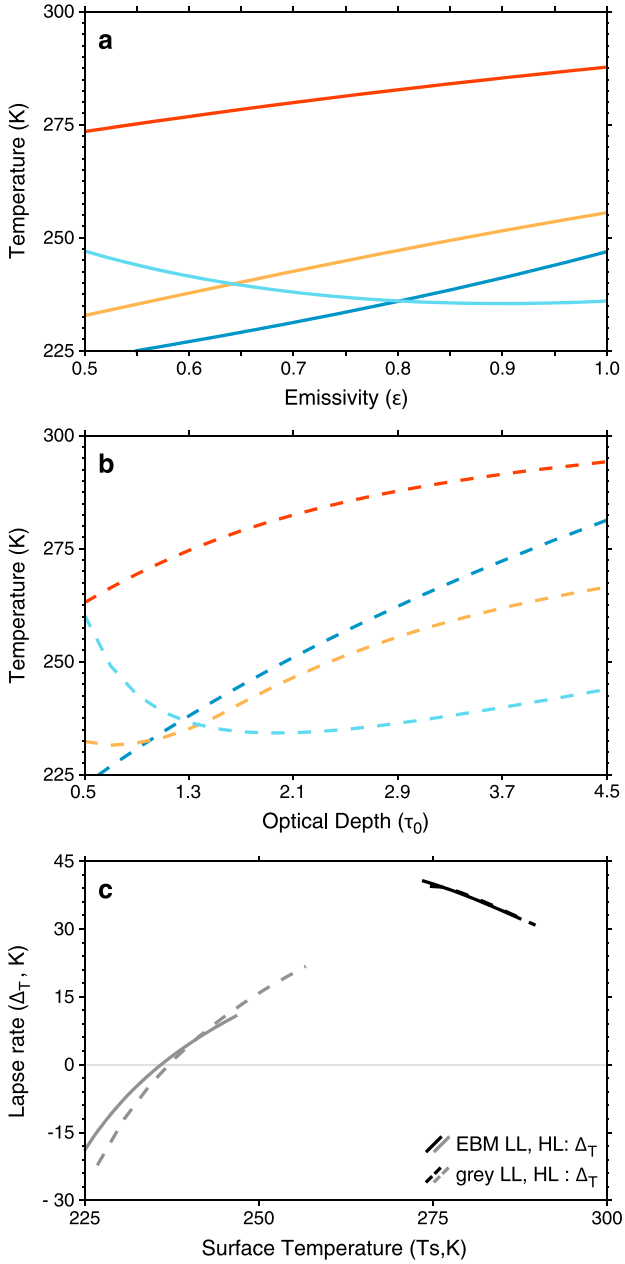

Figure 2. Comparison of the surface (LL, dark orange and HL, dark blue) and atmospheric (LL, light orange and HL, light blue) temperature response to increasing (a) emissivity in the EBM and (b) optical depth in the grey gas model. (c) A direct comparison of the lapse rates ($\Delta_T = T_S - T_A$) for each model (EBM, solid lines and grey gas model, dashed lines) for the high-latitude column (grey) and the low-latitude column (black). In Figure 2c, we also limit the range of optical depths plotted to match the surface temperature range of the EBM; at low latitudes, we show τ_0 = 1.3–3.3, and at high latitudes we show τ_0 = 0.7–2.5.

models is so strong that the atmospheric temperature decreases with increasing optical depth. This limit resembles the stratosphere (also optically thin in the longwave and heated in the shortwave), which also cools in response to increasing greenhouse gas concentrations [*Hansen et al.*, 1997].

We now focus on the sensitivity of the grey gas column to a fixed change in optical depth, $\delta\tau_0 = +0.2$. We select reference-state τ_0 to roughly match present-day high- and low-latitude temperature profiles (compare orange and blue lines to grey lines in Figure 3a), parameterizing differences in total optical depth attributable to differences in column water vapor. We use a reference value of τ_0 = 2.7 at high latitudes and τ_0 = 4.7 at

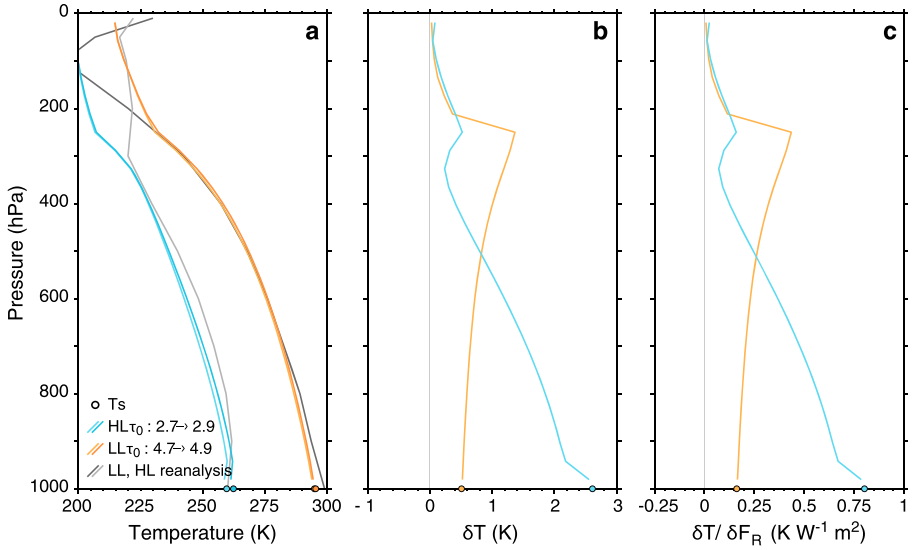

Figure 3. For the grey gas model (a) high-latitude (blue, τ_0: 2.7→2.9) and low-latitude (orange, τ_0: 4.7→4.9) temperature profiles (solid lines) and surface temperatures (filled circles). Grey lines in Figure 3a show reanalysis-derived temperature profiles for the current period (2010–2015). (b) The temperature response for each region. (c) The temperature response normalized by radiative forcing.

low latitudes. These optical depths give $T_S^{LL} = 294.8$ K and $T_S^{HL} = 259.6$ K, with a slight surface inversion and stable troposphere at high latitudes, and a moist adiabatic troposphere at low latitudes.

Figure 3b provides a detailed picture of the lapse rate changes outlined in Figure 2. The temperature sensitivity to a change in optical depth varies vertically and differs between the two regions. High-latitude warming is concentrated in the lower troposphere and at the surface, but low-latitude warming is concentrated in the upper troposphere. Although surface warming is polar amplified, upper tropospheric warming is tropically amplified. This temperature response pattern implies that the meridional temperature gradient weakens at the surface but strengthens in the upper troposphere. The meridional variation in the vertical structure of warming is a robust feature found in previous research [*Meehl et al.*, 2007; *Lu and Cai*, 2010] and would likely lead to changes in poleward atmospheric heat transport [e.g., *Held*, 1978].

Polar amplification inferred from Figure 3b ($\delta T_S^{LL} = 0.6$ K, $\delta T_S^{HL} = 2.8$ K) is much larger than the factor of about 2–3 estimated above. This apparent discrepancy is primarily a result of the regionally differing optical depths assumed in Figure 3 (estimates above assumed similar optical depth in both regions). The radiative forcing in a thick grey atmosphere is approximately proportional to two factors: the relative change of optical depth ($\delta\tau_0/\tau_0$) and the base-state lapse rate. These two factors approximately compensate between regions in Figure 3—$\delta\tau_0/\tau_0$ is larger for high latitudes, but the lapse rate is larger for low latitudes. This compensation makes radiative forcing in the two regions quite similar ($\delta F_R^{LL} = 3.3$ W m^{-2}, $\delta F_R^{HL} = 3.2$ W m^{-2}). Therefore, the warming structure per unit radiative forcing closely resembles the total warming (compare Figures 3c to 3b). To investigate the components of the total temperature feedback, we again calculate the Planck and the lapse rate feedbacks as in section 3.2. The lapse rate feedback is strongly positive at high latitudes ($\lambda_{LR}^{HL} = 1.8$ W m^{-2} K^{-1}) and negative at low latitudes ($\lambda_{LR}^{LL} = -1.8$ W m^{-2} K^{-1}).

To investigate the robustness of our findings, we use the CCM3 model to explore the temperature response to increasing CO_2. We compute the sensitivity to CO_2 doubling for both fixed specific humidity (without water vapor feedback) and fixed relative humidity (with water vapor feedback). For both cases, the reference simulation uses $pCO_2 = 280$ ppmv with relative humidity set to 60% in the troposphere, and specific humidity in the stratosphere set to either the value at the tropopause or 60% relative humidity (whichever is smaller).

Figure 4a shows high- and low-latitude temperature profiles for $pCO_2 = 280$ ppmv and 560 ppmv compared against reanalysis (compare blue and orange lines to grey lines). Model profiles are approximately consistent with reanalysis, with notable differences in the strength of the high-latitude lower tropospheric inversion—an issue we will return to below. As in previous models, the lapse rate increases at high latitudes and decreases at low latitudes for a doubling of CO_2 (Figure 4b). Focusing first on the fixed specific humidity case, we find

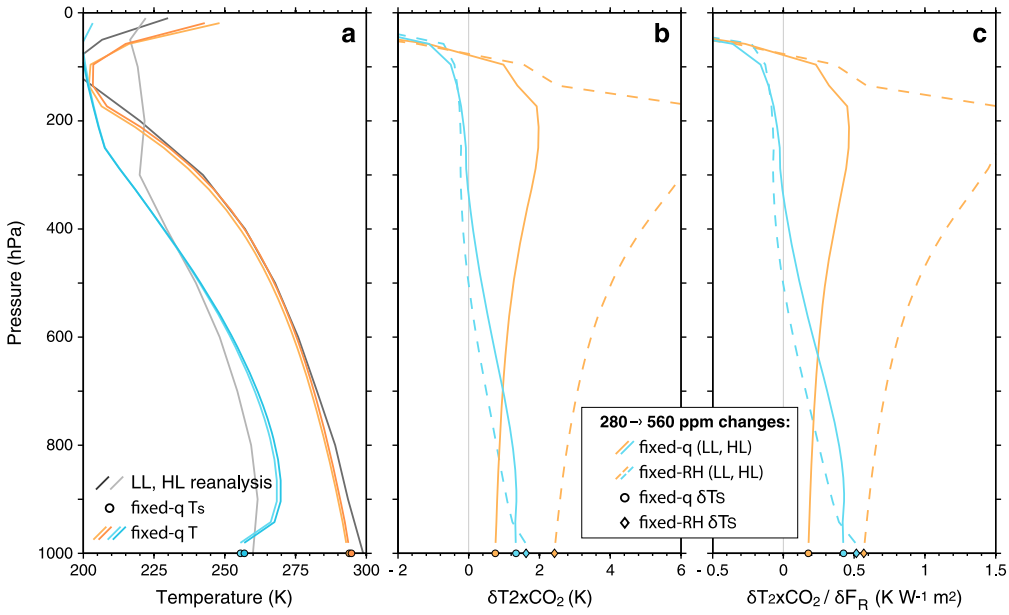

Figure 4. For the CCM3 radiative transfer model (a) high-latitude (blue, CO_2: 280 ppmv → 560 ppmv) and low-latitude (orange, CO_2: 280 ppmv → 560 ppmv) temperature profiles (solid lines) and surface temperatures (filled circles) at fixed specific humidity. Grey lines in Figure 4a show reanalysis-derived temperature profiles for the current period (2010–2015). (b and c) As in Figures 3b and 3c but for CO_2 doubling in two cases: (1) fixed specific humidity (fixed q, solid lines and filled circles) and (2) fixed relative humidity (fixed RH, dashed lines and filled diamonds).

that surface warming is still polar amplified but by a factor of only 1.6 ($\delta T_S^{LL} = 0.8$ K, $\delta T_S^{HL} = 1.3$ K), considerably smaller than in the grey gas model (Figure 3). Part of the decrease in the polar amplification factor owes to a smaller CO_2 forcing at high latitudes compared to low latitudes (stratosphere adjusted [*Hansen et al.*, 1997]; $\delta F_R^{LL} = 4.3$ W m^{-2}, $\delta F_R^{HL} = 3.1$ W m^{-2}), because optical depth in the CO_2 band is increased by the same relative amount in the two regions, but the high-latitude lapse rate is smaller. However, reduced forcing does not fully explain the difference. Comparison of Figures 4c and 3c reveals that the low-latitude sensitivity to radiative forcing is similar between models. However, high-latitude sensitivity depends on the radiation scheme; the grey gas model has greatest sensitivity at the surface, whereas the CCM3 model has greatest sensitivity at 850 hPa. We speculate that this difference is related to the atmospheric window (present only in the CCM3 model)—which allows the surface to radiate directly to space. The presence of a window in the CCM3 model may also lead to the strong high-latitude inversion. Note that we use only clear-sky radiative transfer; including the effects of clouds—which act as grey bodies in the longwave—would likely modify our results.

To investigate the effect of the water vapor feedback, we compare results for fixed specific humidity to a case with fixed relative humidity (compare solid lines to dashed lines in Figure 4). Fixing the relative humidity leads to a strong low-latitude water vapor feedback, canceling the polar amplification seen in previous models ($\delta T_S^{LL} = 2.4$ K, $\delta T_S^{HL} = 1.6$ K; Figure 4b). The water vapor feedback leads to an additional surface warming of 1.6 K for low latitudes but only 0.3 K for high latitudes. The sensitivity of the low-latitude temperature profile to CO_2 doubling is greatly increased by the water vapor feedback (Figures 4b and 4c), and the warming near the tropopause exceeds 6 K. In contrast, there is almost no upper tropospheric warming in the high-latitude profile.

The low-latitude water vapor feedback (estimated by subtracting the total feedback at fixed relative humidity, $\lambda = \delta F_R^{LL}/\delta T_S = 4.3$ W m^{-2}/2.4 K ≈ 1.8 W m^{-2} K^{-1}, from the temperature feedback evaluated at fixed specific humidity: $\lambda_T = \delta F_R^{LL}/\delta T_S = 4.3$ W m^{-2}/0.8 K ≈ 5.4 W m^{-2} K^{-1}) amounts to ~3.6 W m^{-2} K^{-1}, roughly consistent with the tropical clear-sky water vapor feedback in global models [*Soden et al.*, 2008]. However, the all-sky water vapor feedback is generally reduced by 25–50% due to cloud-masking effects (missing in our model). Nevertheless, ignoring additional feedbacks or changes in the heat transport, the water vapor feedback would likely cancel most of the differential effect of the lapse rate feedback, leaving little or no polar amplification.

The robust signal of polar amplification in moist models and paleoclimate records, even in the absence of a surface albedo feedback (which amplifies high-latitude warming), thus indicates the importance of additional processes. One likely candidate is the sensitivity of meridional heat transport to warming. *Hwang and Frierson* [2010] argue that meridional energy transport may to first order be approximated by diffusion of moist static energy. For a given equator-to-pole temperature gradient and relative humidity, the moist static energy gradient increases with warming due to the curvature of the Clausius-Clapeyron relation, thus potentially leading to an increase in the meridional energy transport. Moreover, the temperature change patterns in response to doubling CO_2 (Figure 4b) indicate an enhanced temperature gradient in the atmosphere, as well as a decrease in the high-latitude static stability; both responses may favor further enhanced eddy heat transport [e.g., *Held*, 1978; *Jansen and Ferrari*, 2013]. Investigating the interaction between high- and low-latitude temperature and lapse rate changes and changes in atmospheric heat transport is an important topic for further work but beyond the scope of this article.

5. Conclusions

We analyze the sensitivity of high- and low-latitude surface temperatures to changes in emissivity and radiative forcing using a hierarchy of conceptual models. We show that the differing response of the lapse rate at high and low latitudes results in polar amplification. For fixed lapse rate, surface warming instead depends to first order only on the prescribed lapse rate (and not on the surface temperature). The differential Planck feedback alone, therefore, does not cause polar amplification, as it only compensates for a similarly weaker radiative forcing in response to increased atmospheric emissivity.

Radiative-advective equilibrium solutions provide a base-state model for the high-latitude thermal structure and can be used to explore the atmospheric sensitivity to forcing. The high-latitude atmosphere is stable to convection, with an energy balance between cooling by longwave radiation and the sum of heating by direct solar absorption and atmospheric heat flux convergence. Radiative-advective equilibrium lapse rates are shown to increase strongly in response to surface heating or increasing atmospheric optical depth, leading to a positive lapse rate feedback and amplified surface warming.

Radiative-convective equilibrium is used as a base-state model for the low-latitude thermal structure. The lapse rate is set by moist convection, and the response of the temperature profile to forcing does not depend on the vertical structure of the forcing; the new profile is simply a warmer or colder moist adiabat. The moist adiabatic lapse rate decreases with warming, leading to a negative lapse rate feedback and reduced surface warming.

Our results hold through a hierarchy of idealized column models in the absence of a water vapor feedback. When a water vapor feedback is included, the results for the lapse rate changes hold, but a strong low-latitude water vapor feedback leads to enhanced low-latitude warming, masking the polar amplification caused by meridional differences in the lapse rate response. The lack of polar amplification in the presence of a water vapor feedback occurs only for the present climate and in the limit that clouds, the surface albedo feedback, and changes in atmospheric heat transport are neglected (any of which could restore polar amplification). In warmer climates, the high-latitude water vapor feedback might also have been strong [e.g., *Rose and Ferreira*, 2013]. The destabilization of high-latitude lapse rates in much warmer climates is also important for the onset of high-latitude deep convection [see also *Abbot and Tziperman*, 2008].

Our finding that high-latitude lapse rate changes depend on the nature of the forcing points to limitations of conventional top-of-atmosphere forcing-feedback analyses for understanding high-latitude climate change. If we care about changes in surface temperature, then changes in the atmospheric lapse rate are a critical part of the solution. However, they depend not only on the top-of-atmosphere forcing but also on the vertical structure of that forcing. This finding may be relevant to understanding the role of clouds in high-latitude climate change and their potential ability to alter surface temperature with little or no change in top-of-atmosphere energy balance. Consider, for instance, adding a cloud layer with a negative shortwave δF_S and a positive longwave δF_R that sum to zero; the surface may still warm in response to this cloud layer (see equations (17) and (19)). We hope that future study of radiative-advective equilibrium, in more detailed models that include clouds and variability, will provide further insight into the high-latitude climate and how it responds to forcing.

Acknowledgments
We thank Tim Merlis and an anonymous reviewer for their helpful comments on the manuscript. A.E.P. was supported by a NSF Graduate Research Fellowship (grant DGE-1321846). M.F.J. was supported by a NOAA Climate and Global Change Postdoctoral Fellowship. T.W.C. was supported by a NOAA Climate and Global Change Postdoctoral Fellowship and by the Harvard University Center for the Environment. The presented work started as a summer project during the 2014 Geophysical Fluid Dynamics program at Woods Hole Oceanographic Institution. A.E.P. and M.F.J. gratefully acknowledge support from the GFD program. Reanalysis used in this research is described in *Rienecker et al.* [2011]. Any additional data may be obtained from A.E.P.

References

Abbot, D. S., and E. Tziperman (2008), Sea ice, high-latitude convection, and equable climates, *Geophys. Res. Lett.*, *35*, L03702, doi:10.1029/2007GL032286.

Abbot, D. S., and E. Tziperman (2009), Controls on the activation and strength of a high-latitude convective cloud feedback, *J. Atmos. Sci.*, *66*, 519–529.

Bintanja, R., R. G. Graversen, and W. Hazeleger (2011), Arctic winter warming amplified by the thermal inversion and consequent low infrared cooling to space, *Nat. Geosci. Lett.*, *4*, 758–761.

Caballero, R., J. Mitchell, and M. Steder (2013), CliMT: An object-oriented climate modelling and diagnostics toolkit.

Chylek, P., C. K. Folland, G. Lesins, M. K. Dubey, and M.-Y. Wang (2009), Arctic air temperature change amplification and the Atlantic Multidecadal Oscillation, *Geophys. Res. Lett.*, *36*, L14801, doi:10.1029/2009GL038777.

Graversen, R. G., T. Mauritsen, M. Tjernstrom, E. Kallen, and G. Svensson (2008), Vertical structure of recent Arctic warming, *Nature*, *451*, 53–56.

Graversen, R. G., and M. Wang (2009), Polar amplification in a coupled climate model with locked albedo, *Clim. Dyn.*, *33*, 629–643.

Graversen, R. G., P. L. Langen, and T. Mauritsen (2014), Polar amplification in CCSM4: Contributions from the lapse rate and surface albedo feedbacks, *J. Clim.*, *27*, 4433–4450.

Hall, A. (2004), The role of surface albedo feedback in climate, *J. Clim.*, *17*, 1550–1568.

Hansen, J., M. Sato, and R. Ruedy (1997), Radiative forcing and climate response, *J. Geophys. Res.*, *102*, 6831–6864.

Held, I. M. (1978), The tropospheric lapse rate and climatic sensitivity: Experiments with a two-level atmospheric model, *J. Atmos. Sci.*, *35*, 2083–2098.

Hwang, Y. T., and D. M. W. Frierson (2010), Increasing atmospheric poleward energy transport with global warming, *Geophys. Res. Lett.*, *37*, L24807, doi:10.1029/2010GL045440.

Jansen, M., and R. Ferrari (2013), Equilibration of an atmosphere by adiabatic eddy fluxes, *J. Atmos. Sci.*, *70*, 2948–2962.

Lu, J., and M. Cai (2010), Quantifying contributions to polar warming amplification in an idealized coupled general circulation model, *Clim. Dyn.*, *34*, 669–687.

Manabe, S., and R. T. Wetherald (1975), The effects of doubling the CO_2 concentration on the climate of a general circulation model, *J. Atmos. Sci.*, *32*, 3–15.

Manabe, S., and R. J. Stouffer (1980), Sensitivity of a global climate model to an increase of CO_2 concentration in the atmosphere, *J. Geophys. Res.*, *85*, 5529–5554.

Meehl, G. A., et al. (2007), Global climate projections, in *Climate Change 2007: The Physical Science Basis. Contribution of Warking Group 1 to the Fourth Assessment Report of the Intergovernmental Panel on Climate Change*, edited by S. Solomon et al., Cambridge Univ. Press, Cambridge, U. K., and New York.

Miller, G. H., R. B. Alley, J. Brigham-Grette, J. J. Fitzpatrick, L. Polyak, M. C. Serreze, and J. W. White (2010), Arctic amplification: Can the past constrain the future?, *Quat. Sci. Rev.*, *29*, 1779–1790.

Oort, A. H. (1974), Year-to-year variations in the energy balance of the Arctic, *J. Geophys. Res.*, *79*(9), 1253–1260.

Pithan, F., and T. Mauritsen (2014), Arctic amplification dominated by temperature feedbacks in contemporary climate models, *Nat. Geosci.*, *7*(3), 181–184.

Rienecker, M. M., et al. (2011), MERRA-NASA's Modern-Era Retrospective Analysis for Research and Applications, *J. Clim.*, *24*, 3624–3648.

Roe, G. H., N. Feldl, K. C. Armour, Y. T. Hwang, and D. M. Frierson (2015), The remote impacts of climate feedbacks on regional climate predictability, *Nat. Geosci.*, *8.2*, 135–139.

Rose, B. E., and D. Ferreira (2013), Ocean heat transport and water vapor greenhouse in a warm equable climate: A new look at the low gradient paradox, *J. Clim.*, *26*, 2117–2136.

Serreze, M. C., A. P. Barrett, A. G. Slater, M. Steele, J. Zhang, and K. E. Trenberth (2007), The large-scale energy budget of the Arctic, *J. Geophys. Res.*, *112*, D11122, doi:10.1029/2006JD008230.

Screen, J. A., and I. Simmonds (2010), The central role of diminishing sea ice in recent Arctic temperature amplification, *Nature*, *464*, 1334–1337.

Soden, B. J., I. M. Held, R. Colman, K. M. Shell, J. T. Kiehl, and C. A. Shields (2008), Quantifying climate feedbacks using radiative kernels, *J. Clim.*, *21*(14), 3504–3520.

Trenberth, K. E., and J. M. Caron (2001), Estimates of meridional atmospheric and ocean heat transports, *J. Clim.*, *14*, 3433–3443.

Vavrus, S. (2004), The impact of cloud feedbacks on Arctic climate under greenhouse forcing, *J. Clim.*, *17*, 603–615.

Winton, M. (2006), Amplified arctic climate change: What does surface albedo feedback have to do with it?, *Geophys. Res. Lett.*, *33*, L03701, doi:10.1029/2005GL025244.

Yang, X.-Y., J. C. Fyfe, and G. M. Flato (2010), The role of poleward energy transport in Arctic temperature evolution, *Geophys. Res. Lett.*, *37*, L14803, doi:10.1029/2010GL043934.